Food Materials Research

ARTICLE

Open Access

https://doi.org/10.48130/fmr-0026-0023

Food Materials Research **2026**, 6: e024

Visible-light-responsive Au TOH@TiO_2/sodium alginate composite coatings for postharvest blueberry preservation

Jinge Song[1#], Hui Li[1#], Jiajia Zhang[1], Mingming Ma[2] and Wenjing Yan[1*]

[1] *National Center of Meat Quality & Safety Control, College of Food Science and Technology, Nanjing Agricultural University, Nanjing 210095, China*

[2] *Key Laboratory of Food Contact Materials Safety, State Administration for Market Regulation, Jiangsu Product Quality Testing & Inspection Institute, Nanjing 210007, China*

[#] Authors contributed equally: Jinge Song, Hui Li

[*] Correspondence: ywj1103@njau.edu.cn (Yan W)

Abstract

Blueberries are highly susceptible to microbial spoilage, water loss, softening, and oxidative stress during postharvest storage, which creates an urgent demand for active edible coatings integrating antibacterial and barrier functions. In this study, visible-light-responsive Au trisoctahedra@TiO_2 (Au TOH@TiO_2) core–shell nanocomposites were synthesised and incorporated into sodium alginate (SA) to develop active composite coatings for blueberry preservation. Au TOH@TiO_2 exhibited broad-spectrum photocatalytic antimicrobial activity under LED irradiation: it achieved 100% inactivation of *Staphylococcus aureus* (*S. aureus*), 92.39% growth inhibition of *Escherichia coli* (*E. coli*), and 40.78% mycelial growth inhibition of *Botrytis cinerea* (*B. cinerea*). Incorporation of Au TOH@TiO_2 improved the barrier, mechanical, and antimicrobial properties of SA films. During storage at 25 °C, the 50-SA coating effectively suppressed microbial proliferation and decay, reduced quality deterioration, and better maintained the antioxidant capacity of blueberries compared with the control and pure SA coating. Simple washing procedures greatly reduced Au and Ti residues originating from the composite coatings. These findings suggest that Au TOH@TiO_2/SA composite coatings provide a promising visible-light-responsive active packaging strategy for postharvest blueberry preservation.

Keywords: TiO_2 modification, Visible-light photocatalysis, Sodium alginate composite film, Blueberry preservation

Citation: Song J, Li H, Zhang J, Ma M, Yan W. 2026. Visible-light-responsive Au TOH@TiO_2/sodium alginate composite coatings for postharvest blueberry preservation. *Food Materials Research* 6: e024 https://doi.org/10.48130/fmr-0026-0023

Introduction

Blueberries (*Vaccinium* spp., Ericaceae) are rich in flavonoids, organic acids, vitamins, and other bioactive compounds, but they are highly perishable because of their thin epidermis, soft texture, and high moisture content[1–4]. Mechanical damage during harvesting, handling, and transportation, together with the warm and humid harvest season, can promote juice leakage and microbial proliferation, while postharvest metabolic activity further accelerates water loss, softening, shrivelling, and decay[5–7]. Existing preservation strategies, including low-temperature storage, modified atmosphere packaging, sulfur dioxide-based treatments, physical decontamination, and edible coatings, can delay quality deterioration but are often limited by energy consumption, strict storage requirements, residue-related concerns, or potential adverse effects on sensory quality[8,9]. Bio-based coatings and packaging films offer more sustainable alternatives; however, many conventional systems lack sufficient antimicrobial activity unless functional agents are incorporated[10,11]. Therefore, biodegradable active packaging films that combine barrier properties with antimicrobial functionality are highly desirable for blueberry preservation.

Among various bio-based film-forming materials, sodium alginate (SA), a natural polysaccharide, is particularly attractive because of its outstanding film-forming ability and nontoxicity[12,13]. Nevertheless, SA films generally exhibit limited antimicrobial activity and therefore require functional modification to achieve effective preservation performance[14,15]. Titanium dioxide (TiO_2) has been widely investigated as an inorganic antimicrobial and photocatalytic material for food-related applications. However, TiO_2 possesses a wide band gap that limits its visible-light absorption and photocatalytic efficiency under ambient illumination. Previous studies have shown that coupling TiO_2 with gold (Au) nanostructures can enhance visible-light utilization and facilitate charge separation, thereby enhancing photocatalytic and antimicrobial performance[16].

In this study, gold trisoctahedra (Au TOHs) were used to modify TiO_2 to construct Au TOH@TiO_2 core–shell nanocomposites with enhanced visible-light responsiveness. The nanocomposites were then incorporated into an SA matrix to fabricate SA-based active packaging films. We hypothesized that Au TOH@TiO_2 could enhance visible-light-mediated antimicrobial activity and simultaneously improve the functional properties of SA films. The optical properties, physicochemical characteristics, barrier performance, and *in vitro* antimicrobial activity of the films were systematically evaluated. Blueberries were further used as a model fruit to assess the preservation efficacy of the films during storage, with emphasis on microbial growth, decay incidence, weight loss, and hardness. This work provides a feasible SA-based active packaging strategy for extending the shelf life of blueberries and furnishes experimental evidence for the application of photocatalytic nanocomposites in postharvest blueberry preservation.

Materials and methods

Materials and reagents

Blueberry fruits were uniform in size, with similar maturity and no macroscopic mechanical damage. Chloroauric acid ($HAuCl_4$) was purchased from Sigma-Aldrich Reagents, Inc. (USA). Titanium (IV)

© The Author(s)

https://doi.org/10.48130/fmr-0026-0023

triethanolaminate isopropoxide (abbreviated as TTEAIP), sodium alginate (SA), together with superoxide dismutase (SOD) detection kits, were bought from Shanghai Macklin Biochemical Co., Ltd (China). Other experimental reagents were all supplied at analytical grade purity.

Preparation of Au TOH@TiO_2

Preparation of Au TOHs

Preparation of the Au NP seed suspension was carried out based on the previously published method of Lee et al.[17] and used for the subsequent synthesis of Au TOHs. Au TOHs were synthesised with minor modifications to a previously reported protocol[18]. Briefly, equal volumes of disodium ethylenediaminetetraacetate (EDTA-2Na, 10 mmol/L) solution and $HAuCl_4$ solution (10 mmol/L) were mixed to obtain the precursor solution, which was then diluted 10-fold with ultrapure water. Subsequently, 4 mL of cetyltrimethylammonium chloride (CTAC, 100 mmol/L) aqueous solution was mixed with 3 mL of the diluted precursor solution, followed by the addition of 0.26 mL of freshly prepared ascorbic acid solution (100 mmol/L). After the reaction solution became colourless, 25 μL of the Au NP seed suspension was introduced. The reaction was conducted in a thermostatted shaking incubator at 10 °C, with an agitation rate of 250 rpm for 30 min. The Au TOHs were collected by centrifugation, redispersed in ultrapure water, and stored at 4 °C until use.

Preparation of Au TOH@TiO_2

Au TOH@TiO_2 nanocomposites were synthesized via a slight modification of the method by Atta et al.[19]. Briefly, 1 mL of Au TOH suspension, 19 mL of ultrapure water, and 50 μL of ammonia solution were mixed in a 50 mL conical flask and stirred at 25 ± 2 °C for 30 min. Then, 80 μL TTEAIP was supplemented into the system, and the reaction solution was kept under continuous stirring for 24 h. The resulting Au TOH@TiO_2 nanocomposites were collected by centrifugation at 6,000 rpm for 6 min, washed three times with ultrapure water, and stored until further use.

Characterization of Au TOH@TiO_2

The UV–vis spectra of samples were recorded within the 400–800 nm range for optical property characterization, using ultrapure water as the blank reference. The microscopic morphology and elemental distribution of the nanocomposites were investigated via transmission electron microscopy (TEM) combined with energy-dispersive X-ray spectroscopy mapping (EDS mapping). Hydrodynamic diameter and zeta potential measurements were performed with a nanoparticle size and zeta potential analyzer. For structural characterisation, lyophilised samples were analysed by X-ray photoelectron spectroscopy (XPS), X-ray diffraction (XRD), and Fourier transform infrared spectroscopy (FT-IR). Detailed experimental parameters are available in the Supplementary Text 1.

Visible-light-driven photocatalytic antimicrobial activity of Au TOH@TiO_2

Bacterial activation and antibacterial assay

Escherichia coli (*E. coli*) as well as *Staphylococcus aureus* (*S. aureus*) were incubated in liquid culture medium at 37 °C with a shaking speed of 180 rpm until reaching the logarithmic growth phase. The bacterial cells were collected by centrifugation at 7,000 rpm for 7 min, resuspended in sterile 0.9% saline, and adjusted to 1×10^7 CFU/mL.

For antibacterial assays, 200 μL of bacterial suspension was mixed with 200 μL of Au TOH@TiO_2 suspensions at varying concentrations (13, 19, and 25 mg/mL), and the mixtures were transferred into 48-well plates. Two incubation modes were set up comparatively: dark incubation and visible light irradiation treatment. The visible light source adopted a 30 W white LED lamp with a continuous emission spectrum ranging from 400 to 700 nm (pure visible region, no ultraviolet component). The vertical distance between the lamp source and the surface of sample solutions was fixed at 15 cm, and the average irradiance on the samples was kept consistent throughout the irradiation process. To eliminate thermal interference caused by long-time light exposure, the ambient temperature around the reaction system was maintained steadily, and the temperature rise of bacterial suspensions during illumination was controlled within an acceptable range. The mixtures were incubated for 1, 2, and 3 h under dark conditions or the aforementioned visible light irradiation, respectively. Sterile 0.9% normal saline was used as the blank control group. After treatment, serial gradient dilutions of samples were performed, followed by spreading the diluted bacterial liquid onto agar plates. The plates were cultured at 37 °C for 24–48 h. Finally, the number of viable colonies was counted, and the antibacterial rate was calculated by Eq. (1):

$$\text{Antibacterial rate } (\%) = \frac{N_{control} - N_{treatment}}{N_{control}} \times 100\%, \quad (1)$$

where, $N_{control}$ and $N_{treatment}$ represent the total colony numbers in the control and treatment groups, respectively.

Fungal activation and antifungal assay

Botrytis cinerea (*B. cinerea*) was cultured on potato dextrose agar (PDA) plates at 25 °C for 5–7 d before use. The antifungal activity of Au TOH@TiO_2 was evaluated using the mycelial growth rate method. Briefly, mycelial plugs were excised from the margin of actively growing colonies using a sterile punch and placed, with the mycelial side facing downward, onto the centre of PDA plates containing Au TOH@TiO_2 at different concentrations (13, 19, and 25 mg/mL). The mycelial growth inhibition rate was calculated by Eq. (2):

$$\text{Mycelial growth inhibition rate } (\%) = \frac{D_{control} - D_{treatment}}{D_{control}} \times 100\%, \quad (2)$$

where, $D_{control}$ and $D_{treatment}$ represent the colony diameters of *B. cinerea* in the control and treatment groups, respectively.

Preparation of Au TOH@TiO_2/SA films

SA (2 g) was dissolved in 98 mL of ultrapure water in a constant-temperature water bath maintained at 60 °C. One millilitre of glycerol was added as a plasticiser and mixed thoroughly. Au TOH@TiO_2 suspensions were then incorporated into the SA solution to obtain final Au TOH@TiO_2 concentrations of 0, 12.5, 25, 37.5, and 50 mg/mL in the film-forming systems. The resulting films were designated as SA, 12.5-SA, 25-SA, 37.5-SA, and 50-SA, respectively. The film-forming solutions were degassed by ultrasonication, cast into plastic Petri dishes with a diameter of 90 mm, and dried at 60 °C. A 48-h conditioning treatment at 25 °C and 50% RH was applied to the dried membranes to stabilize their moisture levels.

Characterization of Au TOH@TiO_2/SA films

Thickness, microstructure, and mechanical properties

A digital micrometer accurate to 0.01 mm was adopted to gauge film thickness. Ten random sites on each sample were tested, and the averaged data were recorded. Prior to observation via scanning electron microscopy (SEM), the TOH@TiO_2/SA films were

cryogenically fractured and sputtered with a thin gold layer; this approach allowed visualization of their surface and cross-section microstructures. A universal testing instrument was utilized to characterize the mechanical performance of these membranes. Au TOH@TiO_2/SA films were trimmed into rectangular strips measuring 1 × 4 cm, and tensile tests were conducted with a crosshead speed set at 4 mm/min. Elongation at break (EB) and tensile strength (TS) were calculated based on the recorded stress–strain profiles.

Optical properties, surface wettability, and barrier properties

The visual appearance of the films was recorded using a digital camera, and colour parameters were measured using a colourimeter. Light transmittance was determined using a UV–vis spectrophotometer over the wavelength range of 200–800 nm. Moisture content (MC), water contact angle (WCA), water solubility (WS), water vapour permeability (WVP), oxygen permeability (OP), and carbon dioxide permeability (CO_2P) were measured for the evaluation of physicochemical traits and barrier performance of Au TOH@TiO_2/SA films[20]. Complete experimental parameters can be found in the Supplementary Text 1. The MC was calculated using Eq. (3):

$$\mathrm{MC}\ (\%) = \frac{m_0 - m_1}{m_0} \times 100\%, \tag{3}$$

where, m_0 and m_1 represent the initial mass and dried mass of TOH@TiO_2/SA film (g), respectively.

The WVP was calculated using Eq. (4):

$$\mathrm{WVP}\left(\mathrm{g \cdot mm\ \left(h \cdot m^2 \cdot kPa\right)^{-1}}\right) = \frac{\Delta m \times d}{A \times t \times \Delta P}. \tag{4}$$

The OP and CO_2P were calculated by Eq. (5):

$$\mathrm{OP/CO_2P}\left(\mathrm{g \cdot mm\ \left(h \cdot m^2\right)^{-1}}\right) = \frac{\Delta m \times d}{A \times t}. \tag{5}$$

where, Δm refers to the difference in mass prior to and following the test (g); d is the Au TOH@TiO_2/SA film thickness (mm); A is the permeation area of the TOH@TiO_2/SA film (m^2); t is the testing interval (h); and ΔP is the WVP difference across the TOH@TiO_2/SA film (kPa).

Antibacterial activity of Au TOH@TiO_2/SA composite film-forming solutions

Sterile plate count agar (PCA) medium was mixed with the bacterial suspension at a ratio of 1:100 and poured into sterile Petri dishes. After solidification, 100 μL of film-forming solution was added to each well, with sterile 0.9% saline used as the control. The plates were pre-diffused at 4 °C for 4 h and then incubated at 37 °C under visible-light irradiation using a 30 W LED lamp at a distance of 15 cm or under dark conditions. The inhibition zone diameter was measured using the cross-measurement method.

Blueberry treatment

Blueberries were immersed in 0.3% (v/v) sodium hypochlorite solution for 60 s to reduce surface contaminants and microorganisms. The fruit were then randomly divided into different treatment groups. Blueberries in the control group (CK) received no additional treatment, whereas those in the PE group were wrapped with polyethylene film as a commercial preservation control group. For the SA, 37.5-SA, and 50-SA groups, whole blueberries were immersed in the corresponding film-forming solutions for 60 s and then dried under aseptic conditions. All treated samples were placed in PE packaging boxes and stored at 25 ± 2 °C under visible light irradiation. Blueberry quality attributes were evaluated on days 0, 4, 8, 12, 15, and 18 of storage (Fig. 1).

Determination of blueberry quality attributes

Physical properties, weight loss, decay incidence, and microbial analysis

Microbial populations on blueberry fruit, including the total bacterial count and total yeast and mold counts, were determined by plate counting according to GB 4789.2-2022 and GB 4789.15-2016. Weight loss and decay incidence were determined using 10 fixed fruit from each group at each sampling point. Fruit showing obvious shrivelling, rupture with juice leakage, or visible mold growth were considered decayed. Hardness was measured at the equatorial region of each fruit using a texture analyser. The cylindrical probe, trigger force, test speed, and puncture depth were 5 mm, 0.3 N, 1 mm/s, and 7 mm, respectively.

Determination of nutritional quality, flavour-related attributes, and phytochemical contents

Total soluble solids (TSS) were determined using a digital refractometer after pressing and filtering 5 g of blueberry fruit. Titratable acidity (TA) was measured by acid–base indicator

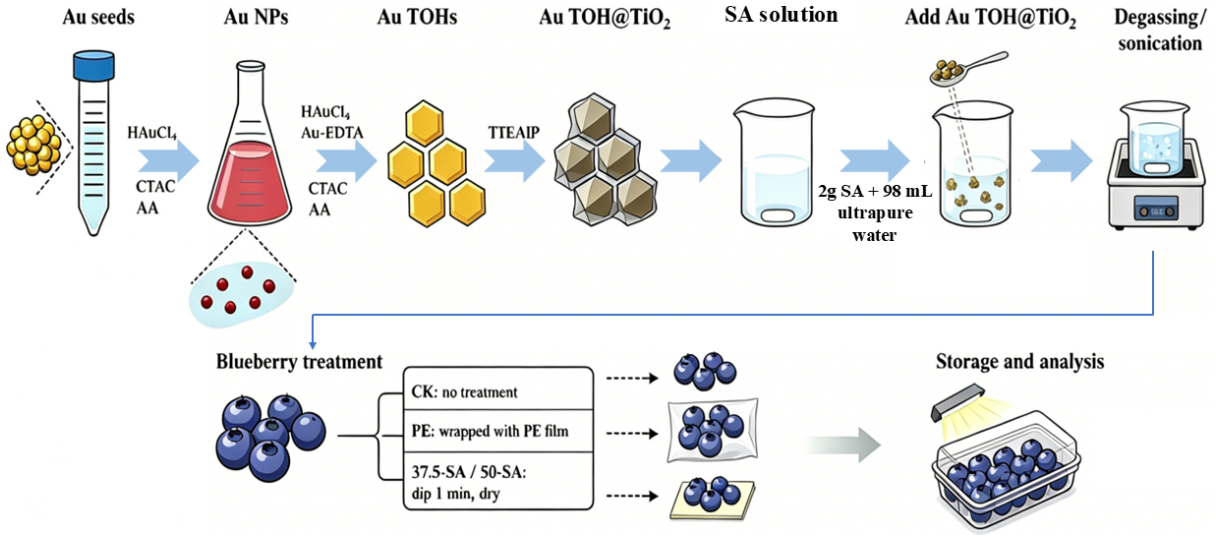

Fig. 1 Schematic illustration of the preparation of Au TOH@TiO_2/SA composite coatings and their application in blueberry preservation.

https://doi.org/10.48130/fmr-0026-0023

titration according to GB 12456-2021. Total phenolics, flavonoids, and anthocyanins were extracted using a precooled 1% HCl–methanol solution and quantified spectrophotometrically at 280, 325, 530, and 600 nm. Detailed extraction procedures are provided in the Supplementary Text 1.

Membrane lipid peroxidation and antioxidant enzyme activity

The thiobarbituric acid method was applied to detect malondialdehyde (MDA) content. After measuring the absorbance of the reaction system at 450, 532, and 600 nm, MDA concentrations were computed based on Eq. (6):

$$C_{MDA}(\mu mol/g) = \frac{[6.45(A_{532} - A_{600}) - 0.560A_{450}] \times V_1}{V_2 \times M}, \quad (6)$$

where, V_1 is the volume of the reaction mixture, V_2 is the total volume of the extract, and M is the mass of the blueberry sample.

SOD activity was measured with a commercially available SOD detection kit in line with the supplier's operational guidelines.

Safety evaluation

Blueberries from the 50-SA group were randomly selected and subjected to three washing treatments: rinsing for 1 min, gentle rubbing for 1 min, and soaking for 5 min. The residual Au and Ti contents on the blueberries' surface were then determined. Unwashed blueberries from the 50-SA group were used as the control to evaluate the potential residue risk associated with the coating treatment.

Statistical analysis

All datasets were processed statistically using IBM SPSS 26.0. Intergroup significant variations were assessed by one-way ANOVA, and Duncan's multiple range test was used for further multiple comparisons. Origin 2018 was adopted for the plotting of all graphs. Error bars denote standard deviation (SD), and distinct lowercase superscript letters mark significant statistical differences at $p < 0.05$.

Results

Characterization of Au TOH@TiO_2

As observed from the TEM images in Supplementary Fig. S1a and S1b, the as-prepared gold nanoparticles exhibited spherical morphology with uniform particle size and favorable dispersibility. The UV–Vis absorption spectrum (Supplementary Fig. S1c) presented an obvious LSPR peak at 521 nm, which verified the successful fabrication of spherical Au NPs. Particle size analysis of the Au NPs aqueous solution (Supplementary Fig. S1d) revealed that the average particle diameter of Au NPs was 9.54 ± 0.19 nm.

The morphology of Au TOHs was characterized using TEM. As displayed in Supplementary Fig. S2a and S2b, the as-synthesized Au TOHs possessed excellent dispersibility and presented a trioctahedral shape with distinct and sharp edges. The UV–Vis absorption spectrum (Supplementary Fig. S2c) exhibited an evident LSPR peak at 548 nm for Au TOHs. According to the particle size distribution histogram (Supplementary Fig. S2d), the average particle size of Au TOHs was calculated to be 60.01 ± 0.69 nm.

It can be seen from the TEM image (Fig. 2a) that the Au TOH core is evenly encapsulated by a TiO_2 shell. According to the particle size distribution histogram of Au TOH@TiO_2 (Fig. 2b), its average particle size was determined to be 115.31 ± 12.30 nm. EDS mapping verified uniform distribution of Au, Ti, and O elements (Fig. 2c; Supplementary Fig. S3). XPS results confirmed metallic Au^0 and Ti^{4+} states, along with Ti–O and Ti–OH bonds in the composites (Fig. 2d). Two characteristic peaks at 82.29 and 85.94 eV observed in the high-resolution Au 4f spectrum can be attributed to Au $4f_{7/2}$ and Au $4f_{5/2}$, which confirms the dominant metallic state of Au (Fig. 2e)[21]. The Ti 2p peaks at 457.05 and 462.76 eV corresponded to Ti $2p_{3/2}$ and Ti $2p_{1/2}$, respectively, confirming the presence of Ti^{4+} (Fig. 2f)[22]. The O 1s peaks at 529.71 and 531.39 eV were attributed to Ti–O and Ti–OH bonds, respectively (Fig. 2g)[23].

The crystalline structure of Au TOH@TiO_2 was further analysed by XRD (Supplementary Fig. S4). The diffraction peaks at 2θ = 38.18°, 44.39°, 64.58°, 77.55°, and 81.72° corresponded to the (111), (200), (220), (311), and (222) crystal planes of cubic metallic Au, respectively[24]. No obvious diffraction peaks of TiO_2 were observed, suggesting that the TiO_2 shell was mainly amorphous[25]. FT-IR analysis showed characteristic O–H, C–H, and Ti–O–Ti vibration bands, further supporting the formation of Au TOH@TiO_2 nanocomposites (Supplementary Fig. S5)[26,27].

Visible-light-driven photocatalytic antimicrobial activity of Au TOH@TiO_2

As shown in Fig. 3a, Au TOH@TiO_2 exhibited concentration- and time-dependent antibacterial activity against *E. coli* under LED irradiation. The antibacterial rate increased with increasing material concentration and incubation time, reaching 92.39% at 25 mg/mL after 3 h of irradiation. The representative colony images further confirmed the marked reduction in viable *E. coli* colonies after photocatalytic treatment (Fig. 3b). In contrast, the antibacterial activity under dark conditions was weaker, with a maximum antibacterial rate of 67.07% under the same conditions (Supplementary Fig. S6), indicating that visible-light irradiation enhances the antibacterial performance of Au TOH@TiO_2. This result is consistent with previous findings on visible-light-activated photocatalytic antimicrobial systems[28]. A similar trend was observed for *S. aureus*. Under LED irradiation, the antibacterial activity of Au TOH@TiO_2 increased progressively with concentration and incubation time (Fig. 3c). Notably, the antibacterial rate against *S. aureus* reached 100% at 19 mg/mL after 3 h and at 25 mg/mL after 2 h. The corresponding colony images showed almost complete suppression of viable *S. aureus* colonies under these conditions (Fig. 3d). By comparison, the antibacterial rates under dark conditions were only 61.89% and 64.01%, respectively (Supplementary Fig. S7), further confirming the light-dependent enhancement of antibacterial activity.

The antifungal activity of Au TOH@TiO_2 was further evaluated against *B. cinerea*. As shown in Fig. 3e, f, Au TOH@TiO_2 inhibited the mycelial growth of *B. cinerea*, with a maximum inhibition rate of 40.78%.

Characterization of Au TOH@TiO_2/SA films

The pure SA film exhibited a relatively smooth and compact surface, whereas the incorporation of Au TOH@TiO_2 slightly increased surface roughness and introduced uniformly distributed granular structures. The cross-sectional images showed that the composite films maintained dense internal structures without phase separation or delamination, indicating compatibility between Au TOH@TiO_2 and the SA matrix (Fig. 4a).

Incorporation of Au TOH@TiO_2 induced remarkable changes in the visual morphology and optical characteristics of the TOH@TiO_2/SA films. The pure SA film was colourless and highly transparent,

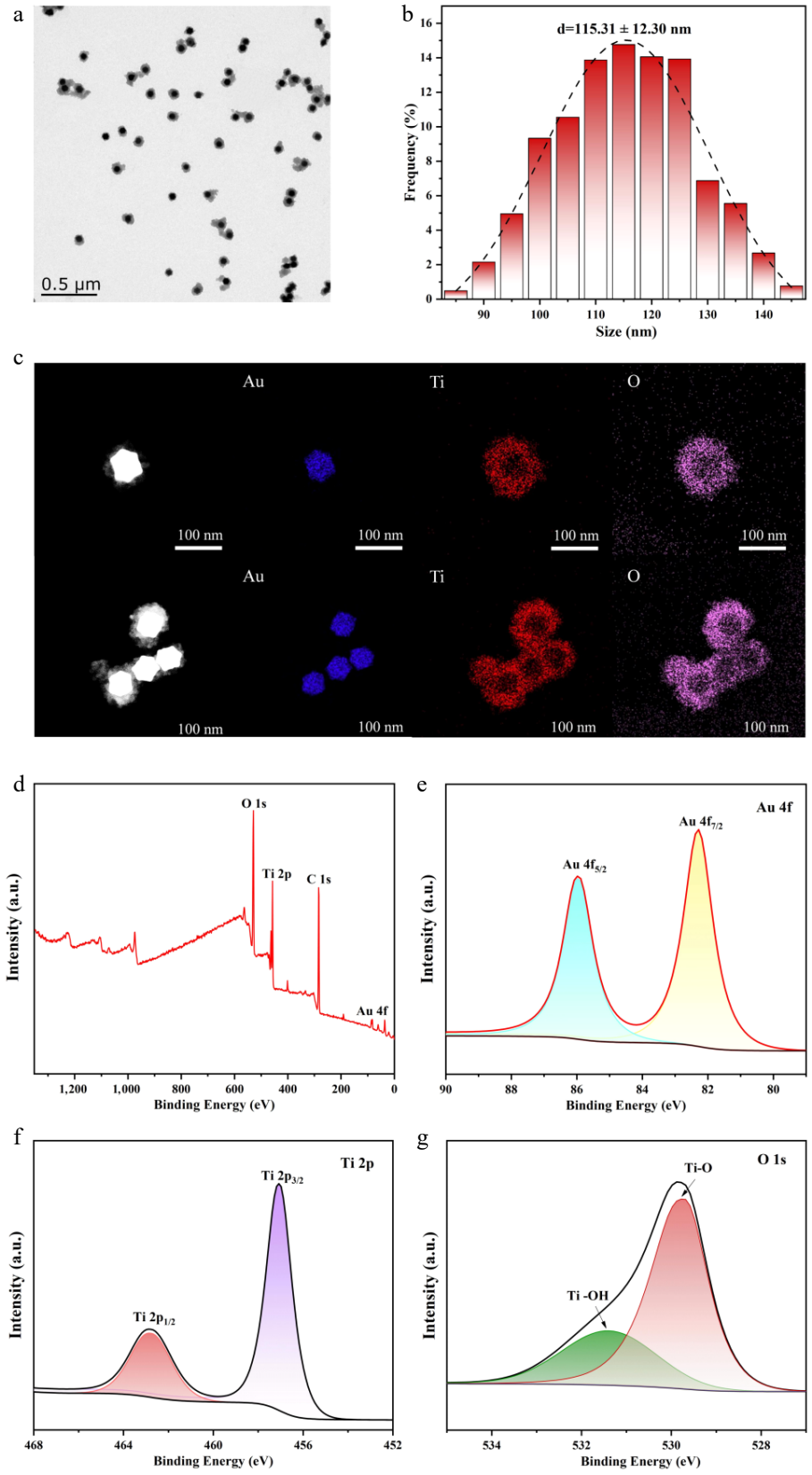

Fig. 2 Characterization of Au TOH@TiO_2. (a) TEM image of Au TOH@TiO_2; (b) particle size distribution histogram; (c) EDS elemental mapping images of Au TOH@TiO_2; (d) XPS survey spectrum of Au TOH@TiO_2; high-resolution XPS spectra of (e) Au 4f, (f) Ti 2p, and (g) O1s.

while the composite films gradually changed from light purple to dark purple with increasing Au TOH@TiO_2 concentration (Fig. 4b). Consistently, the transmittance of the films decreased substantially over the range of 200–800 nm (Fig. 4c). The pure SA film showed

https://doi.org/10.48130/fmr-0026-0023

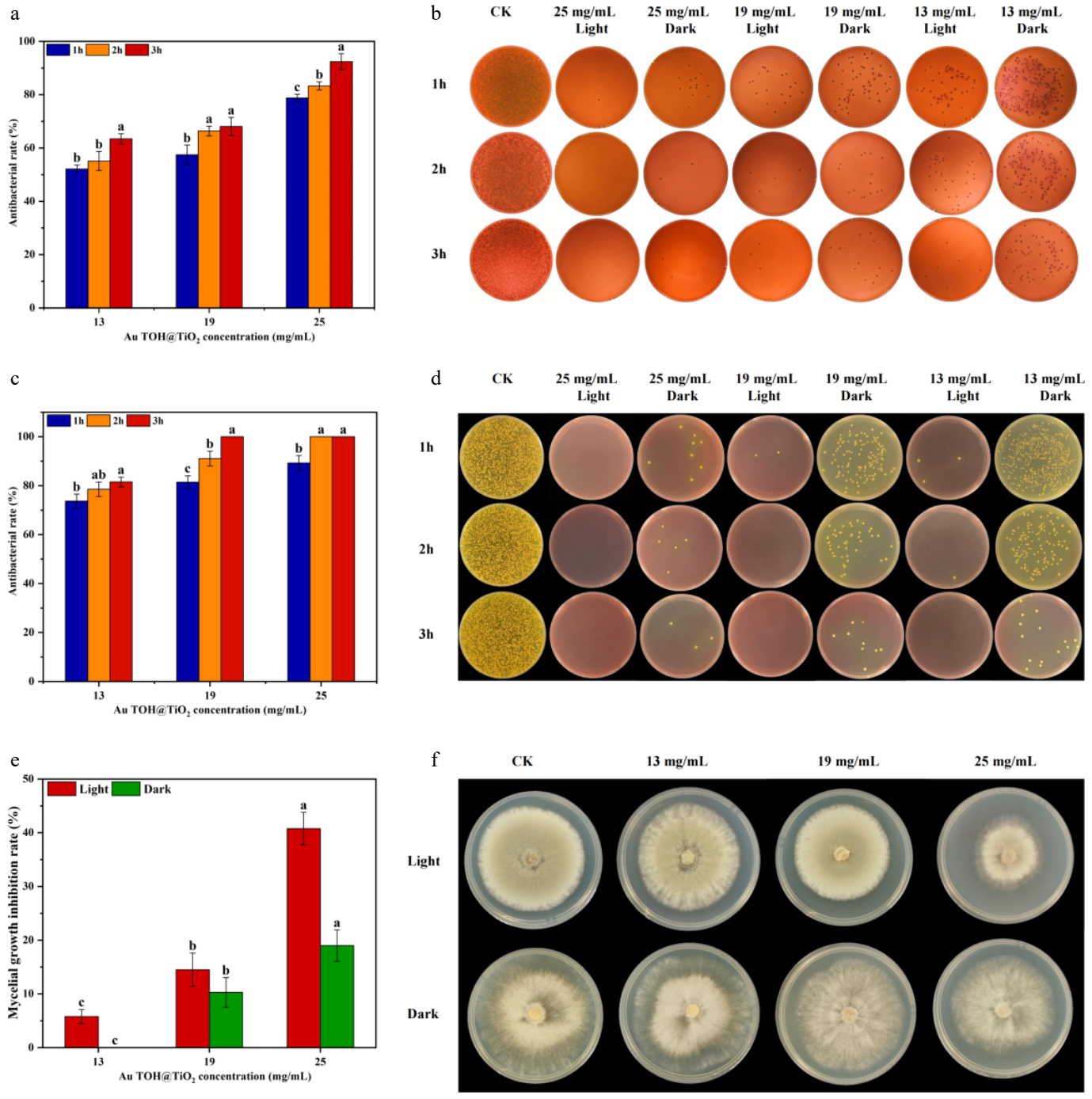

Fig. 3 Photocatalytic antimicrobial activity of Au TOH@TiO_2 against *E. coli*, *S. aureus*, and *B. cinerea*. (a) Antibacterial rates against *E. coli* under LED irradiation; (b) representative colony images of *E. coli*; (c) antibacterial rates against *S. aureus* under LED irradiation; (d) representative colony images of *S. aureus*; (e) mycelial growth inhibition rate of *B. cinerea*; (f) representative mycelial growth images of *B. cinerea*. Different lowercase superscript letters indicate statistically significant differences at the $p < 0.05$ level.

high transmittance, reaching 91.99%, whereas the transmittance of the 50-SA film decreased to 0.15%. In addition, a characteristic absorption band appeared at 550–600 nm, corresponding to the optical response of Au-based nanostructures.

The incorporation of Au TOH@TiO_2 could alter the water-related characteristics of composite films. The MC decreased with increasing nanomaterial concentration, from 41.56% for the pure SA film to 33.45% and 33.20% for the 37.5-SA and 50-SA films, respectively (Supplementary Fig. S8). WS, expressed as dissolution time, increased from 103.81 s for the pure SA film to 134.81 s for the 50-SA film (Fig. 4d), indicating improved water resistance. However, this slower dissolution may limit applications requiring rapid release during fruit and vegetable coating preservation. The WCA results showed that all films remained hydrophilic, although the WCA first increased and then decreased with increasing Au TOH@TiO_2 concentration, reaching a maximum of 47.09° at 25 mg/mL (Supplementary Fig. S9).

The pure SA film exhibited a TS of 42.49 MPa. In comparison, the TS of Au TOH@TiO_2/SA films rose initially and then declined as the Au TOH@TiO_2 loading increased (Fig. 4e).

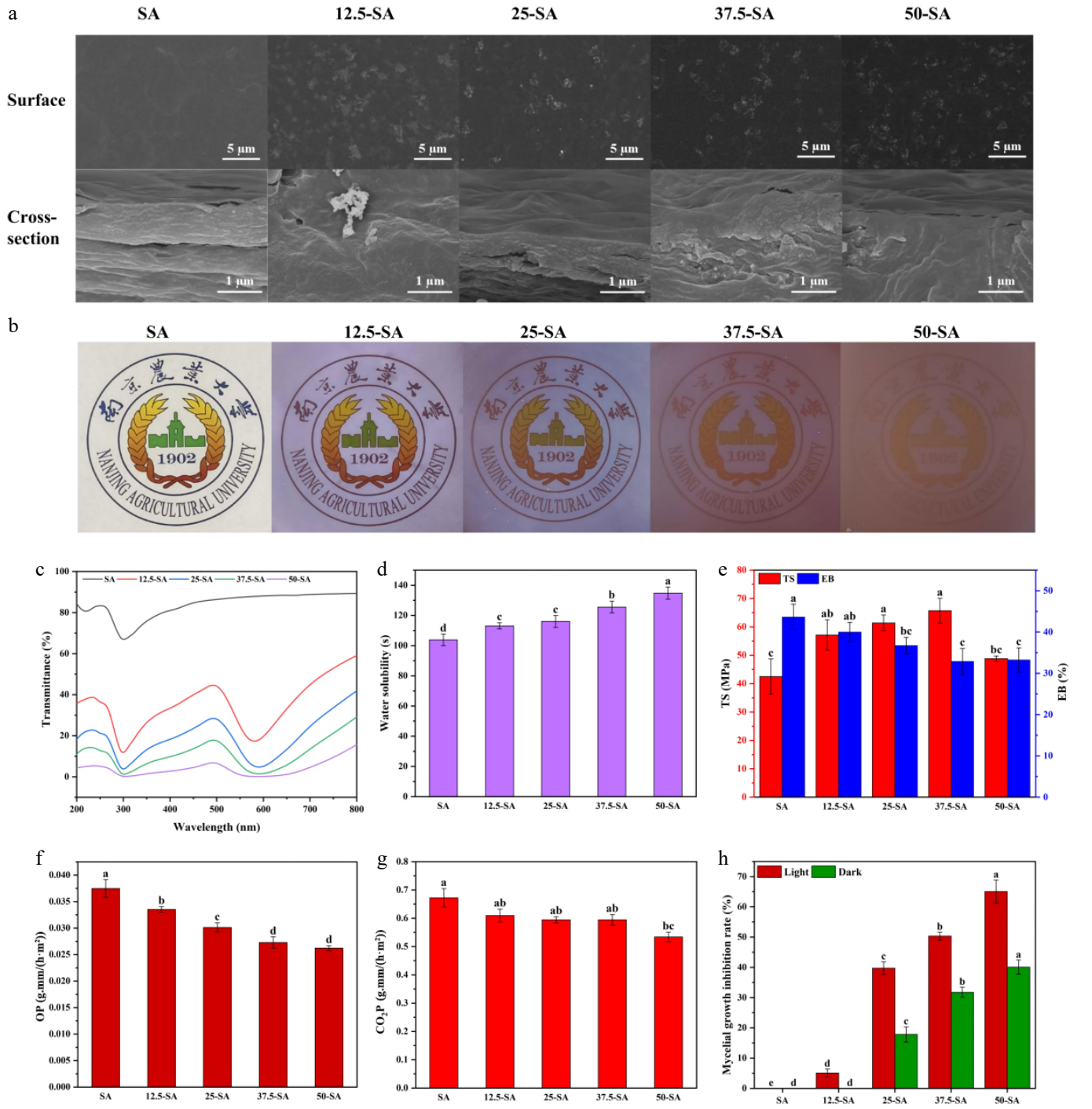

Fig. 4 Characterisation of Au TOH@TiO_2/sodium alginate composite films. (a) SEM images; (b) visual appearance; (c) light transmittance; (d) water solubility (WS); (e) mechanical properties; (f) oxygen permeability (OP); (g) carbon dioxide permeability (CO_2P); (h) mycelial growth inhibition rate of *B. cinerea*.

The WVP first decreased and then increased with increasing Au TOH@TiO_2 content (Supplementary Fig. S10). At suitable concentrations, uniformly dispersed nanoparticles made the Au TOH@TiO_2/SA film structure more compact and extended the diffusion pathway of water vapour molecules, thereby reducing WVP. In contrast, excessive nanoparticle aggregation weakened the compactness of the film and increased WVP again[29]. The OP and CO_2P decreased continuously with increasing Au TOH@TiO_2 concentration (Fig. 4f, g), indicating improved gas-barrier performance.

The pure SA solution showed no obvious antibacterial activity, whereas the Au TOH@TiO_2-containing solutions produced concentration-dependent inhibition zones against *S. aureus* and *E. coli* (Supplementary Table S1; Supplementary Fig. S11). The inhibition zones under light irradiation were larger than those under dark conditions, indicating that Au TOH@TiO_2 endowed the SA matrix with visible-light-responsive antibacterial activity. The antifungal assay against *B. cinerea* also showed clear concentration dependence and light responsiveness (Fig. 4h; Supplementary Fig. S12). At 50 mg/mL Au TOH@TiO_2, the mycelial growth inhibition rate

https://doi.org/10.48130/fmr-0026-0023

reached 65.05% under light irradiation and 40.06% under dark conditions.

Effects of composite coatings on blueberries' appearance and microbial growth

Visual variations of blueberries during 18 days of storage are presented in Fig. 5. On day 12, visible mold contamination was observed on the surface of blueberries in the CK and SA groups, whereas the fruit in the other groups remained visually intact. By day 15, localized mold spots appeared in the PE and 37.5-SA groups. In contrast, visible mold growth was not observed in the 50-SA group until day 18, indicating the strongest antimicrobial and preservation effect. The quantitative microbial analysis further supported these visual observations (Fig. 6a, b). Microbial populations increased continuously in all groups during storage, and differences among treatments became evident from day 4. The total bacterial counts in the CK and SA groups reached 3.82 and 3.87 log CFU/g, whereas that in the 50-SA group was only 3.26 log CFU/g, which was 0.56 log CFU/g lower than that of the CK group. Throughout storage, no significant difference in total microbial counts was observed between the CK and SA groups, indicating that pure SA had no obvious antimicrobial effect. The antimicrobial performance of the 37.5-SA group was comparable to that of the commercial PE film. By day 18, the 50-SA group showed a pronounced antimicrobial advantage. Its total bacterial count was 4.98 log CFU/g, representing reductions of 2.24, 0.91, 2.01, and 0.27 log CFU/g compared with the CK, PE, SA, and 37.5-SA groups, respectively. Similarly, the total mold and yeast counts were reduced by 2.52, 1.28, 2.35, and 0.84 log CFU/g, respectively.

Effects of Au TOH@TiO_2/SA coatings on postharvest quality of blueberries

The variations in physical properties of blueberries under different treatments are displayed in Fig. 6c–e. Weight loss increased continuously during storage, while hardness decreased, reflecting water loss, tissue softening, and senescence progression in blueberries[30]. By day 18, the weight loss of CK and SA reached 18.52% and 16.18%, respectively, whereas that of 50-SA was only 10.91% (Fig. 6c). The decay incidence of CK and SA increased rapidly after day 8 and reached 38.29% and 37.34%, respectively, by day 15; in contrast, the value for 50-SA was 20.14% at the same time point (Fig. 6d). In addition, the hardness of CK decreased from 3.73 to 1.09 N by day 18, while the hardness retention in the 37.5-SA and 50-SA groups was 1.44- and 1.70-fold higher than that of CK (Fig. 6e).

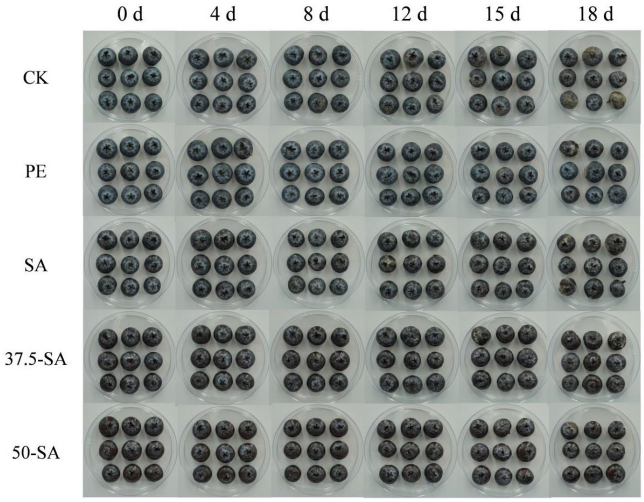

Fig. 5 Effects of Au TOH@TiO_2/sodium alginate composite coatings on blueberry appearance.

TSS and TA are closely related to respiratory metabolism and nutrient consumption during storage. The TSS content first increased and then decreased (Fig. 6f). Compared with CK and SA, PE, 37.5-SA, and 50-SA delayed the peak of TSS and maintained higher levels during the middle and late storage stages. On day 18, the TSS content of 50-SA remained at 10.40%, whereas that of CK decreased to 8.07%. A similar trend was observed for TA (Supplementary Fig. S13), suggesting that the composite coating slowed the consumption of soluble sugars and organic acids.

The antioxidant-related quality attributes are shown in Fig. 7. Flavonoids, total phenolics, and anthocyanins initially increased and then decreased during storage, reflecting a stress-induced accumulation of secondary metabolites followed by senescence-related degradation[31]. Among the treatments, 50-SA most effectively maintained these antioxidant compounds, especially during the middle and late storage stages (Fig. 7b–d). Consistently, the DPPH radical-scavenging activity of 50-SA remained higher than that of CK, reaching 39.45% on day 18 (Fig. 7e). These results indicate that the Au TOH@TiO_2/SA coating helped preserve the non-enzymatic antioxidant capacity of blueberries. Changes in SOD activity and MDA content further reflected the effect of the coatings on oxidative stress and membrane damage. As shown in Fig. 7a, the 50-SA treatment maintained higher SOD activity than CK during the middle and late stages of storage, with an increase of 36.15 U/g fresh weight on day 12. Meanwhile, MDA accumulated continuously in all groups, but its accumulation was lower in coated blueberries. By day 18, the MDA content in CK reached 14.35 μmol/g, whereas that in 50-SA was 11.71 μmol/g (Fig. 7f).

Safety evaluation of the composite coating preservation method

Coating safety is critical to food safety[2]. As shown in Supplementary Table S2, the residual levels of Au and Ti on unwashed blueberries from the 50-SA group were 19,264.79 ± 214.22 μg/kg and 7,200.38 ± 127.83 μg/kg, respectively. After simple washing treatments, both elemental residues decreased markedly. Au and Ti were not detected after rinsing for 1 min or gentle rubbing for 1 min, corresponding to removal efficiencies of 99.99%. Soaking for 5 min also substantially reduced the residual Au and Ti levels to 193.57 ± 0.48 μg/kg and 329.63 ± 7.47 μg/kg, respectively, with removal efficiencies of 98.99% and 95.42%.

Discussion

Characterization of Au TOH@TiO_2

The excellent visible-light responsiveness of Au TOH@TiO_2 was attributed to the unique trisoctahedral Au nanostructure and core–shell configuration. The LSPR effect of Au TOHs broadened the visible-light absorption range and promoted photogenerated charge separation, while the amorphous TiO_2 shell provided abundant photocatalytically active sites. The red shift of the LSPR peak after TiO_2 coating was caused by the changed local dielectric environment, which further optimized visible-light utilization efficiency. The uniform core–shell structure guaranteed stable and sustained photocatalytic activity, laying a foundation for broad-spectrum antimicrobial performance under ambient visible-light conditions.

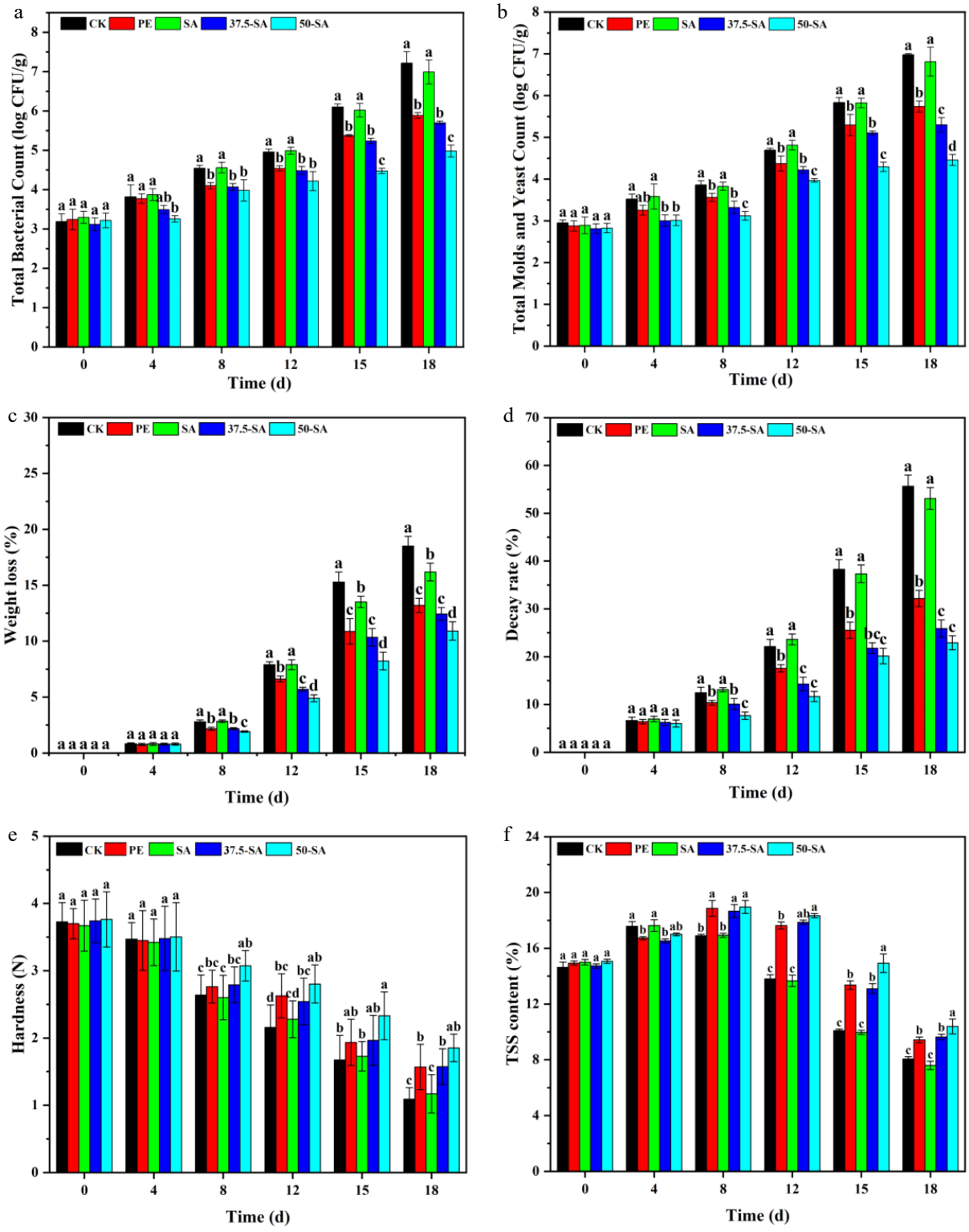

Fig. 6 Effects of composite coatings on microbial growth and physicochemical quality of blueberries during storage. (a) Total bacterial count; (b) total mold and yeast count; (c) weight loss; (d) decay incidence; (e) hardness; and (f) TSS.

Visible-light-driven photocatalytic antimicrobial activity of Au TOH@TiO_2

Compared with the bacterial strains, *B. cinerea* showed lower sensitivity to Au TOH@TiO_2 treatment, suggesting that the antimicrobial efficacy was microorganism-dependent[32]. Au TOH@TiO_2 exhibited broad-spectrum antimicrobial activity, with stronger inhibition against *S. aureus* than against *E. coli* and *B. cinerea*. These results demonstrate the potential of Au TOH@TiO_2 as a visible-light-responsive antimicrobial agent for active food packaging applications[33].

https://doi.org/10.48130/fmr-0026-0023

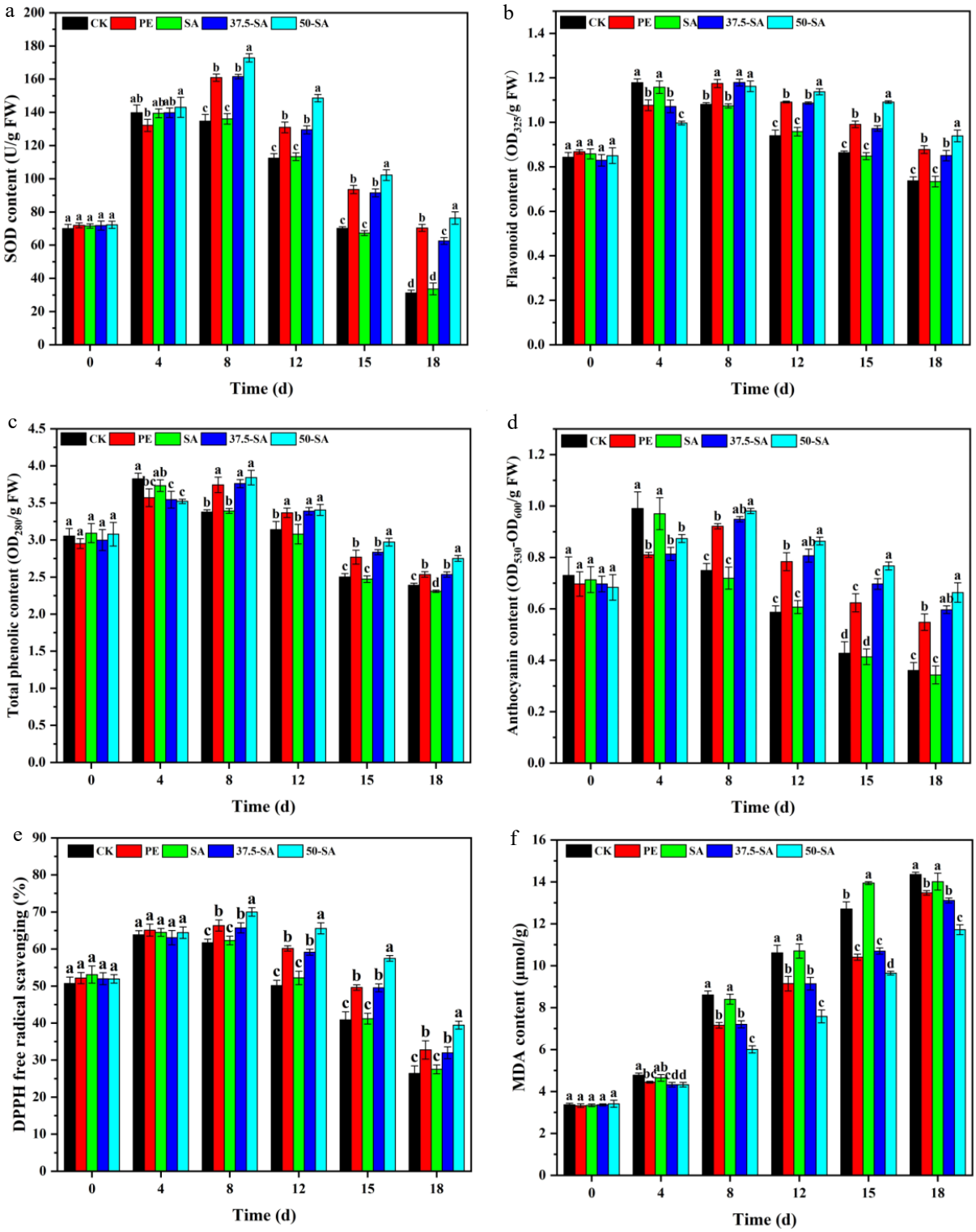

Fig. 7 Effects of composite coatings on antioxidant-related quality attributes of blueberries during storage. (a) SOD activity; (b) flavonoid content; (c) total phenolic content; (d) anthocyanin content; (e) DPPH free radical scavenging activity; and (f) MDA content.

Characterization of Au TOH@TiO_2/SA composite films

Au TOH@TiO_2 nanofillers synergistically improved the comprehensive performance of SA composite films. Moderate nanoparticle addition filled the pores of the SA polymer network, compacted the film microstructure, and thus enhanced mechanical strength and gas barrier properties[34]. The decreased moisture content of composite films can be explained by the pore-filling effect of nanofillers in the SA matrix, which reduces the free volume available for the migration and diffusion of water molecules[35]. The improved gas tortuous diffusion path effectively reduced oxygen and carbon dioxide permeability, alleviating fruit respiratory

metabolism[36]. The changes in light barrier performance are mainly attributed to the enhanced light absorption, scattering, and reflection capacities induced by the incorporated nanomaterials, which greatly reduced light transmittance and endowed the composite films with excellent light-shielding performance[37]. The variation in water solubility can be correlated with the altered surface roughness caused by nanoparticle incorporation[38]. The enhanced antibacterial performance under light irradiation indicates that the fabricated films possessed prominent photodynamic antibacterial effects. However, excessive nanofiller addition caused local aggregation, destroyed film structural continuity, and led to decreased tensile strength[39]. Hydrogen bonding interactions between Au TOH@TiO_2 and SA molecular chains restricted polymer chain movement, resulting in reduced film flexibility and elongation at break[40].

These results demonstrate that Au TOH@TiO_2 incorporation improved the optical, water-resistance, mechanical, gas-barrier, and antimicrobial properties of SA films, supporting their potential application as active food packaging materials.

Preservation mechanism of composite coatings on postharvest blueberries

Visual changes in fruit appearance and quantitative microbial data collectively verified the outstanding preservation superiority of the Au TOH@TiO_2/SA composite coating. Overall, the preservation performance followed the order 50-SA > 37.5-SA ≈ PE > SA ≈ CK. Dynamic changes in soluble solid and organic acid contents were observed throughout storage, which may be associated with the degradation of macromolecules such as starch, cellulose, and pectin during the early storage stage, followed by respiratory consumption during later storage[41,42]. The early occurrence of mold in blank and pure SA groups confirmed that pristine SA lacked effective microbial inhibition ability, which severely limited its preservation capacity under ambient temperature conditions[43]. Compared with commercial PE film and pure SA coating, both the 37.5-SA and 50-SA formulations alleviated microbial spoilage, but the optimized 50-SA coating exhibited the most prominent and durable antimicrobial performance, delaying visible mold growth until the late storage stage. Such dose-dependent photocatalytic activity of Au TOH@TiO_2 under visible light[44,45] also enabled the 50-SA coating to more effectively inhibit decay, weight loss, softening, and oxidative senescence throughout storage, thereby demonstrating superior comprehensive preservation performance and strong practical application potential.

Safety and practical application potential of the coating system

The excellent residue removability confirmed the food safety and practical feasibility of the Au TOH@TiO_2/SA coating strategy. The tightly bound surface residues could be almost completely removed through daily simple washing, avoiding potential heavy metal residue risks. Compared with traditional chemical preservation and commercial PE packaging, this visible-light-responsive edible coating is biodegradable, low-cost, and environmentally friendly, possessing great application potential in postharvest preservation of perishable fruit. Nevertheless, further research is required to clarify the detailed photocatalytic antimicrobial mechanism, evaluate nanoparticle migration behavior, and promote large-scale commercial application.

Conclusions

In this study, visible-light-responsive Au TOH@TiO_2/SA composite coatings were successfully developed for blueberry preservation. Au TOH@TiO_2 exhibited broad-spectrum antimicrobial activity under visible-light irradiation, achieving antibacterial rates of 92.39% against *E. coli* and 100% against *S. aureus*, as well as a maximum mycelial growth inhibition rate of 40.78% against *B. cinerea*. The optimal 50-SA formulation exhibited enhanced physicochemical and antimicrobial properties, and critically, it delivered superior comprehensive preservation effects over commercial PE film and pure SA coating—effectively retarding decay, maintaining nutritional quality, and allowing easy removal of residual nanoparticles by washing. These results underscore the promising application of 50-SA as an advanced active packaging strategy for highly perishable berries. Nevertheless, the detailed photocatalytic antibacterial pathways remain elusive, and only small-scale laboratory tests have been performed; large-scale spraying trials, long-term nanoparticle migration, and cost evaluations are yet to be conducted. Future work will focus on mechanistic elucidation, scaled-up validation, and biosafety assessment to facilitate practical translation.

Author contributions

The authors confirm their contributions to the paper as follows: study conception and design, methodology, draft manuscript preparation: Song J; data collection, writing – review and editing: Li H; analysis and interpretation of results: Zhang J; validation: Ma M; funding acquisition: Yan W. All authors reviewed the results and approved the final version of the manuscript.

Data availability

All data generated or analyzed during this study are included in this published article and its supplementary information files.

Acknowledgments

This work was supported by the National Key Research and Development Program of China (2024YFD2101104), the Key Laboratory of Food Contact Materials Safety, State Administration for Market Regulation (WJ202510R06), and the Jiangsu Provincial Administration for Market Regulation Science and Technology Plan Project (Grant No. KJ2026010).

Conflict of interest

The authors declare that they have no conflict of interest.

Supplementary information accompanies this paper online at: https://doi.org/10.48130/fmr-0026-0023.

Dates

Received 11 July 2026; Revised 6 August 2026; Accepted 6 August 2026; Published online 3 November 2026

References

[1] Xu Y, Chen H, Zhang L, Xu Y. 2023. Clove essential oil loaded chitosan nanocapsules on quality and shelf-life of blueberries. *International Journal of Biological Macromolecules* 249:126091

[2] Du R, Deng J, Huang E, Chen L, Tang J, et al. 2023. Effects of salicylic acid-grafted bamboo hemicellulose on gray mold control in blueberry fruit: the phenylpropanoid pathway and peel microbial community composition. *International Journal of Biological Macromolecules* 251:126303

[3] Tang H, Han Z, Zhao C, Jiang Q, Tang Y, et al. 2023. Preparation and characterization of *Aloe vera* polysaccharide-based packaging film and its application in blueberry preservation. *Progress in Organic Coatings* 177:107445

[4] Vishweshwaraiah YL, Acharya A, Hegde V, Prakash B. 2021. Rational design of hyperstable antibacterial peptides for food preservation. *npj Science of Food* 5:26

[5] Zhou Y, Zhang W, Wu L, Chen P, Li X, et al. 2025. Characterization of fungal pathogens causing blueberry fruit rot disease in China. *Pathogens* 14:201

[6] Lee D, Gwon J, Huang R, Picha DH, Wu Q. 2024. Bio-based nanomaterial suspensions as sprayable coatings for maintaining blueberry postharvest quality. *Food Hydrocolloids* 150:109743

[7] Ren M, Cai Z, Chen L, Wahia H, Zhang L, et al. 2022. Preparation of zein/chitosan/eugenol/curcumin active films for blueberry preservation. *International Journal of Biological Macromolecules* 223:1054–1066

[8] Cao S, Qiao L, Wang X, Huang T, Wu C, et al. 2025. Discussion on postharvest quality, strategies of storage and transportation techniques of blueberries: a comprehensive review. *Food Quality and Safety* 9:fyaf038

[9] Fang Y, Wakisaka M. 2021. A review on the modified atmosphere preservation of fruits and vegetables with cutting-edge technologies. *Agriculture* 11:992

[10] Medina-Jaramillo C, Quintero-Pimiento C, Díaz-Díaz D, Goyanes S, López-Córdoba A. 2020. Improvement of Andean blueberries postharvest preservation using carvacrol/alginate-edible coatings. *Polymers* 12:2352

[11] Li H, Li M, Xu Y, Gao Z, Chi H, et al. 2025. Characterization of excellent performance tea polyphenol-loaded polyethylene oxide/ethyl cellulose nanofiber films prepared by centrifugal spinning and application in blueberry preservation. *Food Bioscience* 71:107376

[12] Baek JH, Lee SY, Oh SW. 2021. Enhancing safety and quality of shrimp by nanoparticles of sodium alginate-based edible coating containing grapefruit seed extract. *International Journal of Biological Macromolecules* 189:84–90

[13] Li S, Fan M, Deng S, Tao N. 2022. Characterization and application in packaging grease of gelatin-sodium alginate edible films cross-linked by pullulan. *Polymers* 14:3199

[14] Li Z, Guo J, Guan F, Yin J, Yang Q, et al. 2023. Oxidized sodium alginate cross-linked calcium alginate/antarctic krill protein composite fiber for improving strength and water resistance. *Colloids and Surfaces A: Physicochemical and Engineering Aspects* 656:130317

[15] Sun J, Wang L, Chen H, Yin G. 2023. Preparation and application of edible film based on sodium carboxymethylcellulose-sodium alginate composite soybean oil body. *Coatings* 13(10):1716

[16] Pakdel E, Daoud WA, Wang X. 2024. Effect of the photoreduction process on the self-cleaning and antibacterial activity of au-doped TiO_2 colloids on cotton fabric. *ACS Applied Materials & Interfaces* 16:25221–25235

[17] Lee S, Fan C, Movsesyan A, Bürger J, Wendisch FJ, et al. 2024. Unraveling the chirality transfer from circularly polarized light to single plasmonic nanoparticles. *Angewandte Chemie (International Edition)* 63:e202319920

[18] Liu S, Zhang J, Yan W. 2024. Controllable synthesis of three-dimensional chiral Au nanoflowers induced by cysteine with excellent biocompatible properties. *Nanomaterials* 14:2040

[19] Atta S, Pennington AM, Celik FE, Fabris L. 2018. TiO_2 on gold nanostars enhances photocatalytic water reduction in the near-infrared regime. *Chem* 4(9):2140–2153

[20] Avramia I, Amariei S. 2022. Formulation of fast dissolving β-glucan/bilberry juice films for packaging dry powdered pharmaceuticals for diabetes. *Plants* 11:2040

[21] Jin K, Qin M, Li X, Wang R, Zhao Y, et al. 2022. Z-scheme $Au@TiO_2/Bi_2WO_6$ heterojunction as efficient visible-light photocatalyst for degradation of antibiotics. *Journal of Molecular Liquids* 364:120017

[22] Ren H, Weng H, Huang J, Lu X, Joo SW. 2022. Synthesis of Au nanoparticle-modified porous TiO_2 nanospheres for detection of toxic volatile organic vapors. *Journal of Alloys and Compounds* 919:165843

[23] Li Z, Chu Y, Mi T, Zhao J, Meng F. 2024. Enhanced photocatalytic H_2 evolution over conjugated polymer/$Au@TiO_2$ ternary heterojunction under visible light: enriched photons input from polymers. *Colloids and Surfaces A: Physicochemical and Engineering Aspects* 692:133991

[24] Zhao L, Niu G, Gao F, Lu K, Sun Z, et al. 2021. Gold nanorods (AuNRs) and zeolitic imidazolate framework-8 (ZIF-8) core-shell nanostructure-based electrochemical sensor for detecting neurotransmitters. *ACS Omega* 6:33149–33158

[25] Chen TM, Xu GY, Ren H, Zhang H, Tian ZQ, et al. 2019. Synthesis of $Au@TiO_2$ core-shell nanoparticles with tunable structures for plasmon-enhanced photocatalysis. *Nanoscale Advances* 1:4522–4528

[26] Hasanzadeh Jeshari H, Rooholamini Nejad H, Saheb V. 2023. Synthesis of reduced graphene oxide coated with $Au@Au_2S$ nanocomposite and study of its photovoltaic properties for use in dye-sensitized solar cells. *Journal of Materials Science: Materials in Electronics* 34:2127

[27] Palusamy S, Jayababu S, Narayanasamy S, Chinnasamy S, Ganesamoorthy T, et al. 2023. A proficient hydrothermally designed Au-$TiO_2/ZnFe_2O_4$ composite for ciprofloxacin removal in wastewater under natural solar light. *Inorganic Chemistry Communications* 156:111317

[28] Uyen NN, Toan NC, Truong N, Tu LA, Le PH. 2025. Plasmonic Au-TiO_2 nanowire/nanotube heterostructures for multifunctional photocatalysis: dye and pesticide degradation, water splitting, and antibacterial activity. *Nanoscale Advances* 7:7317–7332

[29] Hu J, Li D, Huai Q, Geng M, Sun Z, et al. 2023. Development and evaluation of soybean protein isolate–based antibacterial nanocomposite films containing nano-TiO_2. *Industrial Crops and Products* 197:116620

[30] Shi S, Tang J, Zhou Y, Huang H, Zhang J, et al. 2025. Development of sodium alginate-based active packaging films reinforced with curcumin/β-cyclodextrin stabilized high internal phase Pickering emulsions for blueberry preservation. *International Journal of Biological Macromolecules* 321:146365

[31] Xing Y, Yang S, Xu Q, Xu L, Zhu D, et al. 2021. Effect of chitosan/nano-TiO_2 composite coating on the postharvest quality of blueberry fruit. *Coatings* 11:512

[32] Zeng YF, Chen YY, Deng YY, Zheng C, Hong CZ, et al. 2024. Preparation and characterization of lotus root starch based bioactive edible film containing quercetin-encapsulated nanoparticle and its effect on grape preservation. *Carbohydrate Polymers* 323:121389

[33] Lin L, Peng S, Chen X, Li C, Cui H. 2023. Silica nanoparticles loaded with caffeic acid to optimize the performance of cassava starch/sodium carboxymethyl cellulose film for meat packaging. *International Journal of Biological Macromolecules* 241:124591

[34] Xie Q, Liu X, Zhang Y, Liu G. 2023. Development and characterization of a new potato starch/watermelon peel pectin composite film loaded with TiO_2 nanoparticles and microencapsulated *Lycium barbarum* leaf flavonoids and its use in the Tan mutton packaging. *International Journal of Biological Macromolecules* 252:126532

[35] Fonseca JM, Valencia GA, Soares LS, Dotto MER, Campos CEM, et al. 2020. Hydroxypropyl methylcellulose-TiO_2 and gelatin-TiO_2 nanocomposite films: physicochemical and structural properties. *International Journal of Biological Macromolecules* 151:944–956

[36] Wang M, Nian L, Wu J, Cheng S, Yang Z, et al. 2023. Visible light-responsive chitosan/sodium alginate/QDs@ZIF-8 nanocomposite films with antibacterial and ethylene scavenging performance for kiwifruit preservation. *Food Hydrocolloids* 145:109073

[37] Qin Y, Yu H, Chen H, Zhuang Y, Liu Q, et al. 2025. Preparation and characterization of Ag@MOF-*Amomum* tsaoko essential oil/waterborne

polyurethane composite films for strawberry preservation. *Food Control* 178:111533

[38] Liu S, Zhao Y, Xu M, Wen J, Wang H, et al. 2024. Antibacterial photodynamic properties of silver nanoparticles-loaded curcumin composite material in chitosan-based films. *International Journal of Biological Macromolecules* 256:128014

[39] Abaza SF, Elbialy NS, Darwesh R, Mohamed N. 2024. Reinforcing chitosan film with a natural nanofiller "Zein-methyl cellulose loaded curcumin" for improving its physicochemical properties and wound healing activity. *Carbohydrate Polymer Technologies and Applications* 8:100593

[40] Ning Y, Shi J, Yu S, Du R, Ge J, et al. 2024. Characterization of exopolysaccharide/starch composite film incorporated with TiO_2 nanoparticles and its application in chilled meat preservation. *International Journal of Biological Macromolecules* 281:136270

[41] Chen W, Deng J, Wang D, Yang H, Yang J, et al. 2025. Slow-release antimicrobial preservation composite coating based on bamboo-derived xylan–a new way to preserve blueberry freshness. *Food Chemistry* 463:141291

[42] Wang Y, Min S, Gao T, Li C, Ge Y. 2025. Atomized fumigation with basil essential oil regulated reactive oxygen metabolism and respiratory metabolism to maintain storage quality of blueberry fruit. *Postharvest Biology and Technology* 223:113418

[43] Zhao J, Wang Y, Li J, Lei H, Zhen X, et al. 2023. Preparation of chitosan/enoki mushroom foot polysaccharide composite cling film and its application in blueberry preservation. *International Journal of Biological Macromolecules* 246:125567

[44] Motelica L, Ficai D, Oprea OC, Ficai A, Ene VL, et al. 2021. Antibacterial biodegradable films based on alginate with silver nanoparticles and lemongrass essential oil-innovative packaging for cheese. *Nanomaterials* 11:2377

[45] Montes L, Gisbert M, Moreira R. 2022. Water sorption isotherms of different sodium alginates: thermodynamic evaluation and influence of mannuronate-guluronate copolymers. *Journal of Food Processing and Preservation* 46:e17179

Copyright: © 2026 by the author(s). Published by Maximum Academic Press on behalf of Nanjing Agricultural University. This article is an open access article distributed under Creative Commons Attribution License (CC BY 4.0), visit https://creativecommons.org/licenses/by/4.0/.